Advances in Science and Technology Research Journal

Advances in Science and Technology Research Journal, 2026, 20(6), 159–168
https://doi.org/10.12913/22998624/217161
ISSN 2299-8624, License CC-BY 4.0

Received: 2025.12.15
Accepted: 2026.04.15
Published: 2026.05.01

Thermal desorption spectroscopy studies of xenon implanted into germanium

Marcin Turek[1*], Andrzej Droździel[1], Krzysztof Pyszniak[1]

[1] Institute of Physics, Maria Curie Skłodowska University, Pl. M. Curie-Skłodowskiej 1, 20-031 Lublin, Poland
* Corresponding author's e-mail: marcin.turek@umcs.pl

ABSTRACT

The thermal desorption of xenon (Xe) implanted into the germanium (Ge) samples are considered in the paper. The ions of that heavy inert gas are implanted into the target with the energies 100 keV and 150 keV and fluence of 2×10^{16} cm^{-2}. Abrupt emissions of Xe were registered using thermal desorption spectrometry (TDS) in the temperature range 800–840 K. A single TDS peak (width of several K up to ~25 K, depending on heating profile ramp rate) is most probably a result of gas release from pressurized Xe filled cavities formed by vacancy coalescence. The estimated values of the effective activation energy values are: 3.15 eV and 2.1 eV for the implantation energies 100 keV and 150 keV, respectively. These values are comparable to those obtained for Ar and Kr implanted into Ge as well as heavy inert gases in silicon samples.

Keywords: ion implantation, thermal desorption spectroscopy, germanium.

INTRODUCTION

Thermal desorption spectroscopy (TDS) sometimes called a thermal programmed desorption (TPD) is widely used technique for studies of adsorbate (like gases) release from the surface depending on its temperature providing important information about the species present and their reactions on a surface [1]. This method could be easily extended to the release of the implanted species from the subsurface layers of solids (semiconductors, metals, thin layers etc.). Such experiments may give some insight on the lattice defects (like vacancies and their clusters) as well as their kinetics. It could be also helpful in determination of diffusion coefficients [2]. TDS combined with ion implantation could be a direct way to gain knowledge on disorder introduced to lattice by ion impact [3,4]. A very hot topic is the retention of gaseous impurities in materials used both in fission reactors and those planned for future fusion power plants, including Be [5], graphite [6], W [7], zirconium hydride [8], steels [9] and Zr based alloys [10,11]. TDS spectroscopy also helps to gain information on kinetics of chemical reactions on metal surfaces supporting studies on metal corrosion [12].

In its canonical form the TDS spectroscopy measurement involve usually the lightest and most mobile gases like hydrogen, deuterium or helium, but it is not a rule, as the heavy inert gases could also be used. Intense ion implantation with ions of gases may induce lattice disorder and consequently lead to formation of gas-filled cavities and bubbles. Such processes are observed both in metals and in semiconductors. It should be mentioned here that formation of layers containing numerous pressurized gas-filled voids is a crucial step in the ''ion cut'' or ''smart-cut'' thin layer transfer process developed for silicon based electronics by Bruel [13]. A release of He implanted(energy typically 20–50 keV, fluence of the order 10^{16} cm^{-2}) into silicon both from gas-filled cavities and from vacancies was studied also taking the effects of implantation temperatures [14,15]. Evolution of defects in Si was also under investigation via TDS measurements [16]. Both ^{4}He and ^{3}He release was studied after high

fluence implantation with energy in MeV ranges using different annealing regimes [17,18]. Influence of self-ion implantation induced disorder on He release was also reported [19]. It should be mentioned here that release of heavier inert gases, like Ar implanted in low (e.g. 0.1 keV) [20,21] and high energy (50–100 keV) [22,23] into Si, Xe implanted in amorphous or amorphised [24,25] and crystalline Si [26] and even Kr [27] was also under investigation. A general conclusion was achieved that desorption activation energies gets higher as projectile/gas atomic radius and mass increases.

Germanium, which was historically one of the first applied semiconductors attracts again much attention among scientists and engineers due to its higher (compared to Si) carrier mobilities (~3900 $cm^2 V^{-1} s^{-1}$ for electrons and ~1900 $cm^2 V^{-1} s^{-1}$ for holes) which opens new ways for significant performance enhancement of microelectronic and optoelectronic devices, as the miniaturization limit in CMOS technology is about to be reached. SiGe alloys are used in the semiconductor industry to boost the performance of Si-based nanoelectronic devices. As a continuation this alloying approach of group-IV semiconductors, adding Sn was the next step, leading to additional possibilities for tailoring electronic properties [28,29]. Adding Sn enables effective strain and bandgap engineering and can enhance the carrier mobilities, making SiGeSn alloys promising candidates for future opto- and nanoelectronics applications.

It should be also mentioned here that production of subsurface layers containing gas bubbles in germanium or Ge based materials (like eg. SOI wafers) may help to develop a kind of "Smart-cut"-like technique for future Ge electronics. It was demonstrated that 60 keV He^+ ion irradiation with the fluencies of 2×10^{16} cm^{-2} leads to formation of such a layer containing bubbles of ~1 nm in diameter [30]. Moreover, intense H^+ ion beam processing (fluence of the order 10^{17} cm^{-2}) followed by annealing at 200–350 °C resulted in blistering of Ge surface or even led to formation of craters as the implantation fluence was increased [31]. Similar effects were observed also for different regimes (e.g. higher implantation energies) of He and H ion irradiations [32,33]. We presented results of thermal desorption measurements of He [34], Ar [35] and Kr [36] implanted into the crystalline Ge samples with energies 80 keV and 100 keV (He) or 100 and 150 keV (other gases). The fluences were 1×10^{16} cm^{-2} for the lightest projectile and 2×10^{16} cm^{-2} for Ar^+ and Kr^+. We found no signs of surface blistering in all considered cases. The measured helium desorption activation energies were close to 0.75 eV (for the lower temperature peak) while much higher (~3.2 eV and 2.5 eV) for 100 keV Ar^+ and Kr^+, respectively. Desorption activation energies for higher implantation energies were slightly lower (~2.3 eV) for heavier gases. The registered TDS spectra for helium were very broad (with FWHM of 200 K) and consisted of two peaks with centers in the range 700–900 K, shifted by ~100 K. The Ar and Kr releases were of different nature - a single narrow peaks (in the range 790–840 K for Ar, and 800–850 K for Kr) suggest that one deals with sudden release from pressurized and cracking gas-filled bubbles.

The current paper is devoted to investigations of thermal desorption of very heavy noble gas – xenon. One of the aims is to check the release mechanism for such heavy gas – it is expected to be similar to that expected for Kr implanted into Ge or Xe into Si, i.e. a narrow peak suggesting a pressure driven release form gas bubbles. The other issue that should be tested is the value of activation energy for heavy gas release – in the case of implanted Si the activation energies for Ar, Kr and Xe increased with atomic mass of implanted species, while for Ge target activation energies for Kr [36] are lower than for Ar [35]. Moreover, it should be investigated whether in the case of Ge matrix release temperatures for heaviest noble gases increase as in the case of Si, or stay in 750–850 K range as suggested by Ar and Kr measurements. The most abundant isotope (^{132}Xe) was implanted into the germanium target with the energies 100 keV and 150 keV and the same fluencies as for lighter gases (i.e. 2×10^{16} cm^{-2}). The TDS spectra were registered for the linear heating profiles with the ramp rates in the range 0.3 K/s up to 1.5 K/s. The spectra were analysed in order to derive the values of desorption activation energy and the sample surface was checked out to find possible changes of its morphology due to abrupt gas release like exfoliations or crates. The results obtained for Xe are dealt with in the paper and compared to those obtained for other noble gases. A brief description of the experimental apparatus is also included for the sake of completeness.

MATERIAL AND METHODS

Germanium samples (2 inch in diameter, orientation 110) were implanted with Xe^+ ions (A=132) with energies 150 keV and 100 keV. The implantation fluencies 2×10^{16} cm^{-2} were chosen as in the cases of Ar and Kr [35,36]. The irradiations were conducted at room temperature and current density was kept below 1 $\mu A/cm^2$ in order to prevent sample heating. The equipment (i.e. thermal desorption spectrometer, shown in Figure 1) used for collecting spectra was described in several previous papers [19,36]. Nevertheless, a short description is given for completeness sake. The main part of the apparatus is the stainless steel vacuum chamber of ~30 cm in diameter with several flanges and ports attached to it. The chamber contains a sample holder based on the Boralectric HTR1002 (Momentive, Strongsville OH, USA) ceramic-covered heater. The heater module is surrounded by steel and molybdenum screens that prevent the chamber walls from excessive heating as well as help to limit vapour precipitation on internal surfaces of the chamber. The heater is connected to the programmable power supply EA-PS 8080T (EA-Electro-Automatik GmbH, Viersen, Germany), enabling fast and reliable heating up to approximately 1600 K. It is worth mentioning that this limit is mainly due to the usage of the K-type thermocouple for sample temperature measurements. The power supply is controlled by the PC microcomputer with the dedicated custom-made software based on the proportional–integral–derivative (PID) algorithm gaining information from the thermocouple. Both the thermocouple and the power supply communicate with the code via Hewlett-Packard 34970A data acquisition switch. The software enables various heating profiles, however, during all presented measurements there was deployed the linear profile.

The TDS signal (i.e. the partial pressure of the implanted element/isotope) is registered (1 record per second) by the quadruple mass spectrometer QMG 220 M (Pfeiffer Vacuum, Asslar, Germany) controlled by the Quadera™ software package enabling viewing, analyzing the saving the collected spectra. The mass spectrometer is equipped with the secondary electron multiplier detector in order to enhance the detection threshold compared to the early version of the setup, enabling usage of smaller samples (surface typically of the 0.25 cm^2 for faster heating, larger samples for lower ramp rates).

RESULTS

Depth profiles of Xe implanted into Ge and vacancies produced in the target are shown in Figure 2. The profiles were calculated using SRIM simulation software [37] using the quick damage option. The projected implantation ranges were

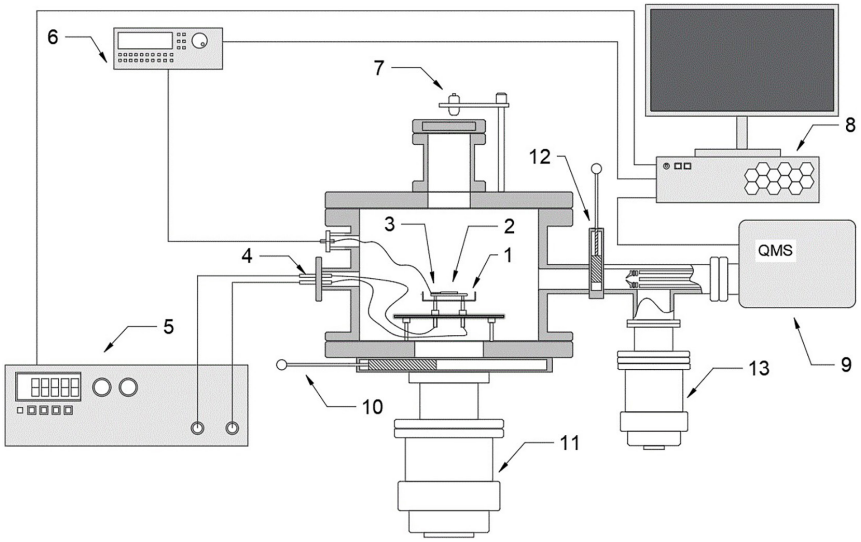

Figure 1. Schematic drawing of the experimental setup: 1 – sample heater, 2 – sample, 3 – K–type thermocouple, 4 – electrical feedthrough (for power supply), 5 – programmable power supply, 6 – data acquisition switch, 7 – optional pyrometer, 8 – PC–class microcomputer, 9 – quadruple mass spectrometer, 10, 12– gatevalves, 11, 13– turbomolecular pumps

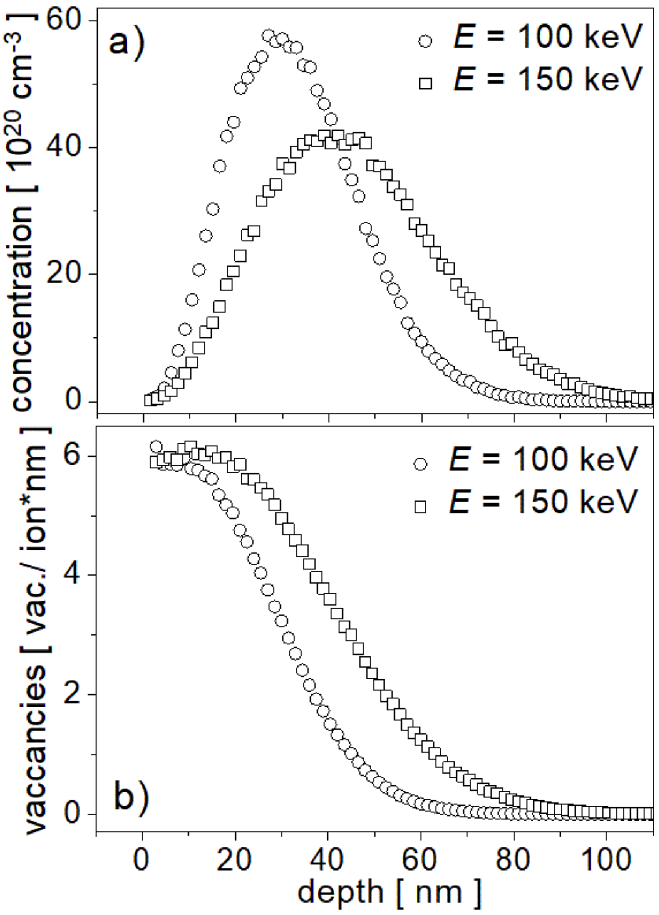

Figure 2. Depth profiles of Xe (a) implanted into germanium with energies 100 keV and 150 keV and produced vacancies (b)

32 nm (100 keV) and 45 nm (150 keV) with the stragglings 20 nm and 14 nm, respectively. As one may expect, the implantation ranges are shorter than in the case of Kr implanted into Ge [36]. Consequently, the maximum dopant and vacancy concentrations are higher by ~50%.

The defected Ge subsurface layer thickness is ~ 20 nm. Unlike in the case of Ar or He [34,35] one does not deal with a thin unmodified layer covering the defected one, the thin both defected and implanted layer lies very near to the surface.

The registered thermal desorption spectra are shown in Figures 3 and 4. As in the case of Ar and Kr one deals with single, rather narrow peak that suggest the release of Xe form bubbles. The fluences of Xe implantations were twice as high as for He, and the projected ranges are shorter nearly 15 times. Consequently, much larger Xe concentration combined with much more intense production of defects, leads to creation of gas-filled cavities. These cavities are formed due to the coalescence of vacancies or their small clusters, sometimes containing trapped Xe atoms. As in the case of Ar and Kr [35,36], an abrupt emission of Xe is registered as the critical pressure in the bubble is achieved due to the rising temperature. The similar effect was also seen for or heavy noble gases implanted into Si [26,27].

During all presented measurements the linear profile was deployed:

$$T(t) = T_o + \beta t \tag{1}$$

where: T_o is the initial (i.e. room) temperature and β is the heating ramp rate. The release of Xe from the germanium samples is detected in the temperature range 800–840 K for both implantation energies, which is more or less the same as in the case of Ar or Kr measurements, yet lower than in the case of He implanted with E = 100 keV.

The most plausible release mechanism in the considered case is the release from pressurized gas-filled bubbles, suggested by a single narrow peak in the measured curves. This is consistent with

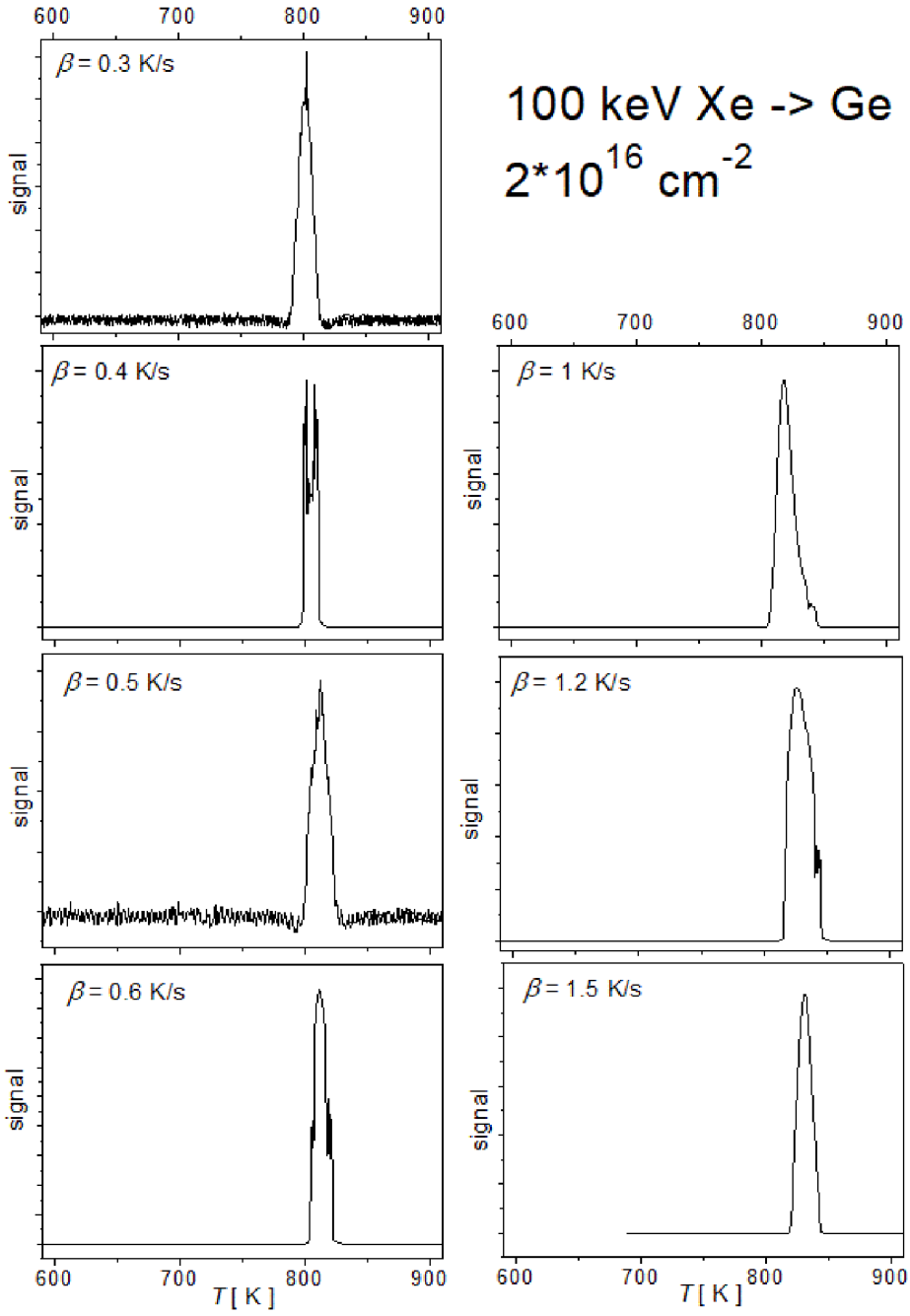

Figure 3. TDS spectra for Xe implanted into Ge with energy E=100 keV

previous results for other heavy noble gases, but it must be clearly stated that it is not yet confirmed by any additional e.g. microstructural studies such as electron microscopy, providing information on bubble size or its distribution. One should have in mind that the width of these peaks is noticeably larger than in the case of Ar and Kr. The FWHM values reach even ~25 K especially for higher heating ramp rates. This is especially well visible in Figure 4 – one can see that peak width for β = 0.3 K/s is below 10 K and increases for faster heating rates. The width of the release peak could be a sign of larger spread in bubble size distribution. Larger width for faster heating, especially well visible for deeper implantation may point at larger spread of bubble size distribution, which could be also related for stronger temperature gradient on the sample during the faster heating. Another reason for registering of wider peaks in the case of faster heating is purely equipment related. One should keep in mind that temperature axis in Figures 3 and 4 is also a scaled measurement time axis. Assuming constant pumping speed during all measurements one deals with a widening of peaks according to Equation 1.

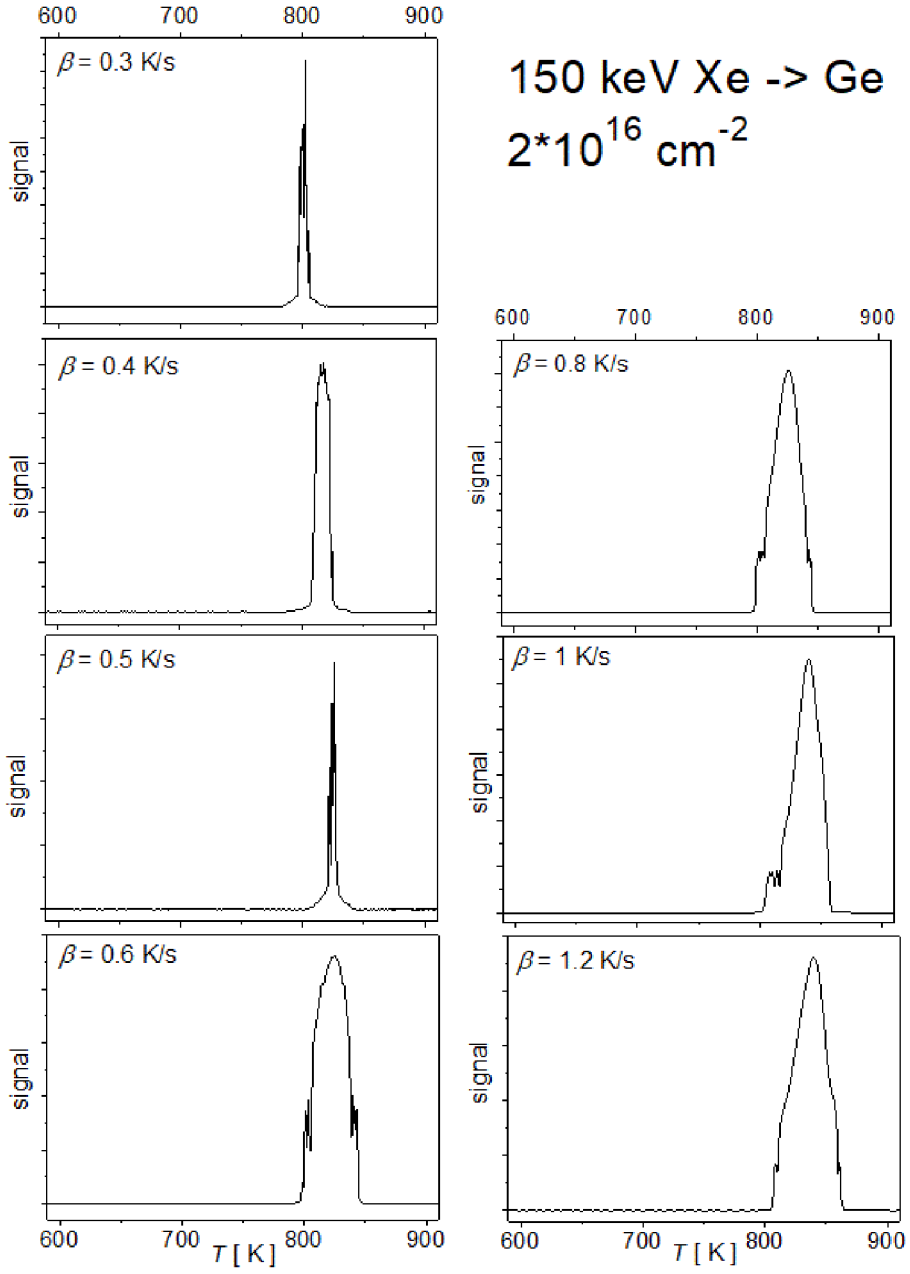

Figure 4. TDS spectra for Xe implanted into Ge with energy E=150 keV

Analyzing the spectra in Figures 3 and 4 and having in mind the data shown in Table 1. one can observe that the peak positions for Xe release peaks are shifted towards higher T as the heating ramp rate β increases, which is a typical behaviour.

These shifts are comparable to that measured for Kr and Ar implanted into Ge [35,36], and approximately two times smaller than for He in germanium target - in that case the shift by ~70 K when ramp rate β was increased from 0.45 K/s up to 1.5 K/s).

The peak position differences for E=150 keV and E=100 keV are larger than for Kr or Ar, reaching values up to 20 K. Nevertheless, these shifts are still much smaller than those of He (~70 K) in the considered ramp rate range. It should be kept in mind that peak shifts for the mentioned irradiation energies for Xe implated into silicon reached values of several hundreds of kelvins.

Estimation of the desorption activation energies could be done applying peak shift analysis proposed by Redhead [38]. The desorption process kinetics could be described by Polanyi-Wigner equation:

$$\frac{dn}{dt} = -\gamma(n,T)n^m \exp\left(-\frac{Q(n,T)}{kT}\right) \qquad (2)$$

In the formula above n is the surface density of the desorbing particles, m is the kinetic order of the process, k is the Boltzmann constant, Q is the desorption activation energy and γ is some pre-exponential factor. The Redhead approach is applicable for the first order (m=1) processes and under assumption and both the pre-exponential factor γ and the desorption energy Q do not depend on n. In such case the Polanyi-Wigner is simplified to the form:

$$\frac{dn}{dt} = -\gamma n \exp\left(-\frac{Q}{kT}\right) \tag{3}$$

Keeping in mind that dn/dt is proportional to the measured TDS signal, which achieves its peak value (denoted as T_p) when $d^2n/dt^2 = 0$ is fulfilled and taking in to account that one deals with linear heating profile (1) one may get the relation:

$$\frac{1}{T_p} = \frac{k}{Q}\ln\left(\frac{T_p^{\,2}}{\beta}\right) + \frac{k}{Q}\ln\left(\gamma\frac{k}{Q}\right) \tag{4}$$

As can bee easily seen in from the above equation, the diffusion activation energy Q could be obtained by deriving the slope of the $1/T_p$ vs. $\ln(T_p^{\,2}/\beta)$ plot. The Redhead approach is widely applied scheme for interpretation of various TDS spectra, it should be kept in mind that the sudden release from pressurized gas bubbles (the most probable release mechanism in the considered case) differs much from diffusion driven first order desorption like observed for He as broad peaks. On the other hand, the processes that result in bubble formation, i.e. vacancy coalescence, gas particle diffusion etc. may be assumed to be described by first order kinetics. Hence, the activation energy values should be treated *cum grano salis* as effective parameters describing the whole release process rather than desorption barriers.

Table 1. Peak positions (Tp) for different heating ramp rates _beta_ and the values of desorption activation energies Q calculated according to Redhead approach

E [keV]	β [K/s]	T_p [K]	Q [eV]
100	0.3	801	3.15 ± 0.25
	0.4	804	
	0.5	811	
	0.6	812	
	1	818	
	1.2	825	
	1.5	830	
150	0.3	800	2.1 ± 0.3
	0.4	816	
	0.5	824	
	0.6	825	
	0.8	826	
	1	838	
	1.2	840	

The Redhead plots for the considered case are presented in Figure 5. The slopes of the straight lines that were fitted to experimental data obtained for the two irradiation energies differ a little: the slope for E=150 keV is larger. The obtained estimated values of the desorption activation energy are shown in Table 1. The desorption activation energy for E=100 keV is 3.15 eV ± 0.25 eV and 2.1 eV ± 0.3 eV for that for E=150 keV. It could be shown that desorption and gas diffusion is strongly affected by the amount of disorder introduced into the matrix. Higher degree of disorders results in higher concentration of traps and scattering centers that hinder that process, resulting in broadening of release peaks and sometimes increase of effective activation energy, depending on defect-gas atom binding energy. Such effect as was observed for He in defected Si [19] and for Ar implanted into Ge [35]. Effective activation energy lower by ~1 eV for 150 keV implanted Xe compared to the 100 keV case could be interpreted looking at the damage distribution profiles in Figure 2. Vacancy concentration at Xe peak position for E=100 keV is by ~30 % higher than that for E=150 keV. It should be also mentioned here that for the previously considered case of Kr implanted into Ge the corresponding concentrations were very similar and so was effective activation energy values, taking into account estimation errors.

These Q values are comparable to that obtained for Ar implanted into Ge [35]. For Kr (E =100 keV) released form the same matrix the desorption activation energy was by ~1 eV higher than both for Ar and Xe, which is rather surprising. This could be an effect of superposition of two opposed trends. The first of them is an increase of activation energy with the size of diffusing atom from Ar (calculated atomic radius ~71 pm) through Kr (~ 88 pm) up to Xe (~108 pm). The second aspect is increasing concentration of the implanted gas due to reduction of the projected range with the projectile mass. Higher

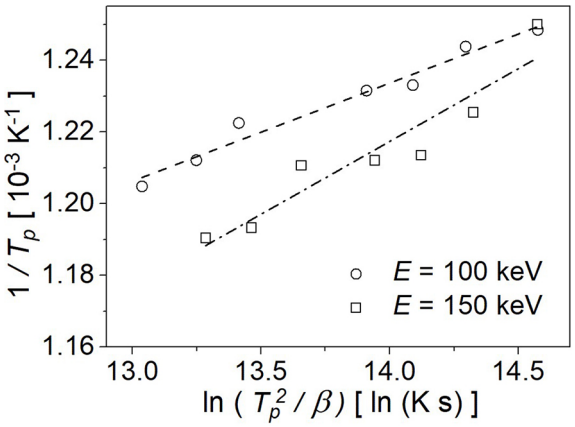

Figure 5. Redhead plot for the TDS spectra presented in Figures 3 and 4

concentration may result in easier formation of gas bubbles at the pre-release stage.

To summarize up, in the case of Ge desorption activation energies are much higher for Ar than for He, but any further essential growth of Q is observed with the mass of heavier noble gases. It should be reminded that for Si one deals with constant increase of activation energies and release temperatures with mass of the noble gas projectile and (what could be even more important) its atomic radius.

CONCLUSIONS

In the paper the investigation of thermal desorption of Xe implanted into germanium samples with energies 100 keV and 150 keV is presented. The implantation energies are the same as for previously considered lighter noble gases. One has to keep in mind that for the heavy projectile the implantation ranges are by factor 2–3 shorter than for Ar implanted into germanium, which leads to larger concentration of the implanted particles. The thermal desorption spectra were collected for linear heating profiles with ramp rates changing form 0.3 up to 1.5 K/s. During each measurement a single, rather narrow Xe emission peak was registered with a center in temperature ranging from 800 K up to 840 K (the same range as for Ar and Kr in Ge). The sudden Xe emission is most probably the effect of the release of the gas trapped into pressurized bubbles, created as a result of vacancy clusters coalescence. It must be, however clearly stated that this explanation, based on similarity of desorption spectra in other cases, is not directly proven by any additional studies, e.g. microstructural ones. The peak shift analysis according to Redhead approach allowed estimation of desorption activation energy. It should be also kept in mind that using Redhead provides values of activation energy only in the case of first order processes. For other orders, as for sudden release from gas bubbles, these estimations should be taken with caution, as effective parameters describing the whole gas migration/bubble formation/release process. Having due regard for this, the effective activation energy values were approximately 2.1 eV ± 0.3 eV for E=150 keV and 3.15 eV ± 0.25 eV for E=100 keV, values similar to those determined for Ar implanted into Ge samples.

REFERENCES

1. Chittenden C.N., Pylant E.D., Schwaner A.L., White J.M. Thermal Desorption Mass Spectrometry. In: Hubbard A.T. (Ed.) The Handbook of Surface Imaging and Visualization. CRC Press, Boca Raton; 1995.
2. Pisarev A., Giniyatullin B. Influence of true diffusion coefficient on hydrogen diffusion in tungsten in the field of defects. Journal of Physics: Conference Series; 2019; 1370: 012061. https://doi.org/10.1088/1742-6596/1370/1/012061
3. Ogura S., Fukutani K. (Eds.) Thermal Desorption Spectroscopy. In: The Surface Science Society of Japan. Compendium of Surface and Interface Analysis. Springer, Singapore; 2018. https://doi.org/10.1007/978-981-10-6156-1_116
4. Kantre K., Szabo P.S., Moro M.V., et al. Combination of in-situ ion beam analysis and thermal desorption spectroscopy for studying deuterium implanted in tungsten. Physica Scripta; 2021; 96:124004. https://doi.org/10.1088/1402-4896/ac1a88
5. Makepeace C., Pardanaud C., Roubin P., et al. The effect of beryllium oxide on retention in JET ITER-like wall tiles. Nuclear Materials and Energy; 2019; 19:346-351. https://doi.org/10.1016/j.nme.2019.02.022
6. Zhang M., Deng K., Wei F., Wu X., Du L., Liu W. Adsorption and desorption of tritium on/from nuclear graphite. ACS Omega; 2022; 7(1):752-760. https://doi.org/10.1021/acsomega.1c05395
7. Oya M., Shimada M., Taylor C.N., et al. Deuterium retention in tungsten irradiated by high-dose neutrons at high temperature. Nuclear Materials and Energy; 2021; 27:100980. https://doi.org/10.1016/j.nme.2021.100980
8. Ma M., Liang L., Tang B., et al. Decomposition kinetics study of zirconium hydride by interrupted thermal desorption spectroscopy. Journal of Alloys

and Compounds; 2015; 645:S217-S220. https://doi.org/10.1016/j.jallcom.2015.01.054

9. Oo K.Z., Chernov I.I., Staltsov M.S., et al. Thermal desorption of helium from reactor steel. Atomic Energy; 2011; 110:151–159. https://doi.org/10.1007/s10512-011-9404-6
10. Sypchenko V.S., Nikitenkov N.N., Tyurin Y.I. Thermal desorption of hydrogen from titanium, zirconium alloy Zr–1% Nb, and the thin-film Ti/Zr–1% Nb system. Journal of Surface Investigations; 2022; 16:870–875. https://doi.org/10.1134/S1027451022050354
11. Juillet C., Tupin M., Martin F., et al. Effect of a pre-oxidation on the hydrogen desorption from Zircaloy-4. Corrosion Science; 2020; 173:108762. https://doi.org/10.1016/j.corsci.2020.108762
12. Karimi S., Taji I., Palencsár S., et al. Evaluation of microstructural and environmental effects on hydrogen uptake and desorption in high-strength carbon steels: A thermal desorption spectroscopy study. Corrosion Science; 2023; 219:111210. https://doi.org/10.1016/j.corsci.2023.111210
13. Bruel M., Aspar B., Charlet B., et al. "Smart cut": a promising new SOI material technology. IEEE International SOI Conference Proceedings; 1995; 178–179. https://doi.org/10.1109/SOI.1995.526518
14. Cerofolini G.F., Calzolari G., Corni F., et al. Thermal desorption spectra from cavities in helium-implanted silicon. Physical Review B; 2000; 61:10183. https://doi.org/10.1103/PhysRevB.61.10183
15. Oliviero E., David M.L., Beaufort M.F., Barbot J.F., van Veen A. On the effects of implantation temperature in helium implanted silicon. Applied Physics Letters; 2002; 81:4201–4203. https://doi.org/10.1063/1.1525059
16. Corni F., Calzolari G., Gambetta F., et al. Evolution of vacancy-like defects in helium-implanted (100) silicon studied by thermal desorption spectrometry. Materials Science and Engineering B; 2000; 71:207–212. https://doi.org/10.1016/S0921-5107(99)00376-1
17. Godey S., Ntsoenzok E., Sauvage T., et al. Helium desorption from cavities induced by high energy 3He and 4He implantation in silicon. Materials Science and Engineering B; 2000; 73:54–59. https://doi.org/10.1016/S0921-5107(99)00433-X
18. Desgardin P., Barthe M.-F., Ntsoenzok E., Liu C.-L. Modifications of He implantation induced cavities in silicon by MeV silicon implantation. Applied Surface Science; 2006; 252:3231-3236. https://doi.org/10.1016/j.apsusc.2005.08.080
19. Turek M., Droździel A., Pyszniak K., et al. Thermal desorption of helium from defected silicon. Acta Physica Polonica A; 2015; 128:849–852. https://doi.org/10.12693/APhysPolA.128.849
20. Lau W.M., Bello I., Huang L.J., Feng X., Vos M., Mitchell I.V. Argon incorporation in Si(100) by ion bombardment at 15–100 eV. Journal of Applied Physics; 1993; 74(12):7101–7106. https://doi.org/10.1063/1.355024
21. Filius A., van Veen A., Bijkerk K.R., Evans J.H. The retention of Ar in low energy high fluence Ar-irradiated Mo and Si. Radiation Effects and Defects; 1989; 108(1):1-8. https://doi.org/10.1080/10420158908217864
22. Hanada R., Saito S., Nagata S., Yamaguchi S., Shinozuka T., Fujioka I. TDS and RBS studies of Ar implanted into Si. Materials Science Forum; 1995; 196–201:1375-xxx. https://doi.org/10.4028/www.scientific.net/MSF.196-201.1375-1380
23. Drozdziel A., Wojtowicz A., Turek M., et al. Thermal desorption studies of Ar+ implanted silicon. Acta Physica Polonica A; 2014; 125(6):1400–1403. https://doi.org/10.12693/APhysPolA.125.1400
24. Werner M., van den Berg J.A., Armour D.G., et al. Shallow BF2 implants in Xe-bombardment-preamorphized Si: the interaction between Xe and F. Applied Physics Letters; 2005; 86(15):151904. https://doi.org/10.1063/1.1900305
25. Barbieri P.F., Landers R., Marques F.C. Electronic and structural properties of implanted xenon in amorphous silicon. Applied Physics Letters; 2007; 90(16):164104. https://doi.org/10.1063/1.2723072
26. Turek M., Droździel A., Pyszniak K., Wójtowicz A., Vaganov Y. Termodesorpcja ksenonu implantowanego do krzemu (in Polish). Przegląd Elektrotechniczny; 2018; 94(7):157–161. https://doi.org/10.15199/48.2018.07.40
27. Turek M., Droździel A., Pyszniak K., et al. Thermal desorption of krypton implanted into silicon. Acta Physica Polonica A; 2017; 132(2):249–253. https://doi.org/10.12693/APhysPolA.132.249
28. Steuer O., Michailow M., Hübner R., et al. Si1−x−yGeySnx alloy formation by Sn ion implantation and flash lamp annealing. Journal of Applied Physics; 2024; 136:065701. https://doi.org/10.1063/5.0220639
29. Wang M., Shaikh M.S., Li Y., et al. Charge transport in n-type As- and Sb-hyperdoped Ge. Applied Physics Letters; 2024; 124:142107. https://doi.org/10.1063/5.0192944
30. David M.-L., Alix K., Pailloux F. In situ controlled modification of the helium density in single helium-filled nanobubbles. Journal of Applied Physics; 2014; 115:123508. https://doi.org/10.1063/1.4869213
31. Yang F., Zhang X.-X., Ye T.-C., Zhuang S.-L. The investigation on surface blistering of Ge implanted by hydrogen under low-temperature annealing. Journal of The Electrochemical Society; 2011; 158(12):H1233. https://doi.org/10.1149/2.065112jes

32. Chien C., Chao D., Liang J., Lin C. Investigation of surface blistering and exfoliation in germanium induced by hydrogen molecular ion implantation. ECS Transactions; 2012; 44:759–766. https://doi.org/10.1149/1.3694395
33. Dai J.Y., Wei X., Xue Z.Y., Di Z.F., Zhang M. Order and temperature dependence of surface blistering in H- and He-co-implanted Ge. Thin Solid Films; 2014; 557:115-119. https://doi.org/10.1016/j.tsf.2013.11.024
34. Turek M., Droździel A., Pyszniak K., et al. Thermal desorption of He implanted into Ge. Acta Physica Polonica A; 2019; 136:285–289. https://doi.org/10.12693/APhysPolA.136.285
35. Turek M., Droździel A., Pyszniak K., Prucnal S., Żuk J., Węgierek P. Termodesorpcja argonu implantowanego do germanu (in Polish). Przegląd Elektrotechniczny; 2020; 96(8):126–130. https://doi.org/10.15199/48.2020.08.25
36. Turek M., Droździel A., Pyszniak K., Prucnal S., Żuk J., Węgierek P. Thermal desorption of Kr implanted into germanium. Acta Physica Polonica A; 2022; 142:776–782. https://doi.org/10.12693/APhysPolA.142.776
37. Ziegler J.F., Ziegler M.D., Biersack J.P. The stopping and range of ions in matter. Nuclear Instruments and Methods B; 2010; 268:1818–1823. https://doi.org/10.1016/j.nimb.2010.02.091
38. Redhead P.A. Thermal desorption of gases. Vacuum; 1962; 12:203–211. https://doi.org/10.1016/0042-207X(62)90978-8